RHESSI ASPECT RECONSTRUCTION

M. FIVIAN, R. HEMMECK, A. MCHEDLISHVILI and A. ZEHNDER
Paul Scherrer Institute, CH-5232 Villigen PSI, Switzerland

(Received and accepted 20 September 2002)

Abstract. The Reuven Ramaty High-Energy Solar Spectroscopic Imager RHESSI spacecraft spins at about 15 rpm around an axis close to Sun center. Precise knowledge of the pointing and the roll angle of the rotating spacecraft is needed in order to reconstruct images with 2 arc sec resolution using the modulation patterns seen on each of the detectors behind the bi-grid rotating collimators. Therefore, the aspect system consists of two subsystems of sensors, the Solar Aspect System (SAS) and Roll Angle System (RAS). The measured data are sent to the Aspect Data Processor (ADP), where a data compression of about a factor of 1000 and a formatting into telemetry packets takes place. The transmitted data consist of 'solar limb' data from the SAS and 'star event' data from the RAS. Knowing the geometry of all features of the SAS, the position of the Sun center, with respect to a spacecraft fixed coordinate system, can be reconstructed. Similarly, a list of position angle marks can be generated by fitting of the star events and subsequent comparison with a star catalog. Integrating this information allows correcting and interpolating the roll angles that provides a precision of < 0.4 arc sec (pitch and yaw) and < 1 arc min (roll).

1. Introduction

The Reuven Ramaty High-Energy Solar Spectroscopic Imager RHESSI is a Small Explorer mission that was launched by NASA on 5 February 2002 into a circular orbit (600 km altitude, 38 deg inclination). The primary scientific aim of the mission is to investigate the physics of particle acceleration and energy release in solar flares. RHESSI observes the full Sun with an unprecedented combination of spatial resolution (as fine as 2.3 arc sec) and energy resolution (1 keV to 5 keV) in the energy range from 3 keV to 17 MeV. The single instrument on a spin stabilized spacecraft utilizes Fourier-transform imaging with 9 bi-grid rotating modulation collimators spaced at 1.55 m and 9 cooled germanium detectors (Lin *et al.*, 2002).

Since the transmission probability for a photon through the collimators depends on the incident angle with respect to the telescope axis (Hurford *et al.*, 2002), and because the spacecraft can only be controlled on an arc-min level, the spatial resolution depends critically on a precise knowledge of the instantaneous pointing direction and roll angle. In order to have a spatial resolution of 2.3 arc sec (for the finest grid) and to precisely correlate with observations at other wavelengths, two precise aspect systems are implemented, the Solar Aspect System (SAS) and the Roll Angle System (RAS). The SAS yields sub-arc sec knowledge of the radial pointing with respect to Sun center and the RAS provides precise knowledge on the roll angle of the rotating spacecraft (about 15 rpm). The combined SAS/RAS

Solar Physics **210:** 87–99, 2002.
© 2002 *Kluwer Academic Publishers. Printed in the Netherlands.*

aspect system provides a knowledge of the absolute pointing with an accuracy of 1 arc sec.

There are two totally independent instruments on RHESSI measuring the roll angle. At one stage of the development of the RHESSI hardware, the schedule and some performance uncertainties of the roll angle system (RAS) motivated the team to add a redundant roll sensor as a backup system. The latter, the Photo-Multiplier Tube Roll Angle System (PMTRAS), is based on a photo-multiplier tube and is described by Hurford and Curtis (2002). In many aspects, the two instruments are complementary (Hurford and Curtis, 2002). Nevertheless, the RAS is measuring the polar angle of every star event and therefore the RAS data can also be used to reconstruct solar off-pointing for non-solar science. As it turned out, both RAS and PMTRAS are operational, but initial RHESSI imaging has been based on the PMTRAS.

The design and the alignment of the RHESSI imager, i.e., the telescope tube with the grids and the SAS/RAS aspect optics and sensors are discussed by Zehnder *et al.* (2002) and only a short overview is given in the next section. The current status of the calibration of the aspect system is reported by Fivian, Henneck, and Zehnder (2002). In this paper, the aspect data processing and the reconstruction of the aspect solution are presented.

2. The Design of the Aspect Systems

A pair of widely separated grids in front of a cooled Ge detector (Smith *et al.*, 2002) produces the characteristic intensity modulation. Each grid consists of a planar array of equally spaced, X-ray-opaque slats separated by transparent slits. If the slits of each pair of grids are parallel to each other and if their pitches (p) are identical, then the transmission is modulated depending on the direction of the incident X-rays. For slits and slats of equal width, the transmission is modulated from zero to 50% and back to zero for a change $a = p/L$, where L is the separation between the grids. The angular resolution is then defined as $p/(2L)$.

The efficiency of the modulation for each of the 9 collimators depends critically on the alignment of the corresponding grid pair. In particular, the finest grids with a pitch of 34 μm must always be aligned within 20 arc sec in twist ($r_{\text{Grid}} \times \Delta\Phi \ll p/2$, with twist $\Delta\Phi$ and r_{Grid} radius of grid). Another necessary ingredient for image reconstruction with a resolution as high as 2.3 arc sec is the accuracy of the measurement of the pointing with respect to the collimators. Therefore, a structure had to be found which guaranteed the stability of the collimators and the aspect systems throughout the integration procedure, the launch and the thermal stress over the orbit (Zehnder *et al.*, 2002). In addition, the definition of the coordinates for measuring the pointing have to be chosen in such a way that the axis of the collimators can always be measured with respect to Sun center fulfilling the requirements in accuracy.

2.1. SOLAR ASPECT SYSTEM (SAS)

The SAS is a set of 3 identical lens/sensor subsystems. Each subsystem consists of a 4 cm diameter lens located on the front grid tray of the imager tube. Each lens focuses a solar optical image onto a 2048-element $\times$ (13 μm)^2 linear CCD located on the rear grid tray. The orientation of the three linear CCDs are equally spaced at 120 deg. The focal length, given by the length of the imager tube, is 1.55 m resulting in a plate scale of 1.73 arc sec pixel^{-1}. In order to reduce chromatic aberration, a bandpass filter at 670 nm with 12 nm bandwidth (FWHM) has been used.

In principle, the measured Sun pointing is related to the SAS features only. In order to have the measurements immune to bending of the imager tube, a design has been chosen to have the lenses coplanar with the front grids and the CCDs coplanar with the rear grids.

While each of the three CCDs are sampling solar profiles at 128 Hz using a programmable integration time between 0.02 and 2 ms, the digitized signal is sent to the Aspect Data Processor (ADP) where a hardware-programmed algorithm triggers one or several pixels around the solar limb using an adjustable threshold. The amplitudes of typically 4 pixels for each of the 6 limbs are written to the telemetry packets using 8 or 10 bits precision.

Each SAS sensor is running with a constant cycle timing at 128 Hz. Within every cycle of $\approx$ 8 ms, the sunlight is integrated on the pixels of the CCD. The accumulated charge is shifted out with a frequency of 1 MHz and sampled twice, once at the offset level and once at the signal level. The subsequent digitization at the 12-bit ADC (analog digital converter) provides a resolution of 0.5 mV channel^{-1} (2 V/2^{12}channels $\approx$ 0.5 mV channel^{-1}). To remove the charge of the continuously incident sunlight the readout of the CCD follows a pre-readout that removes most of the charge accumulated during off-integration time. The front-end electronics incorporates a Field Programmable Gate Array (FPGA) providing basic control of the sensor. In the normal operational mode, the difference of the two samples is calculated and bits 1–10 are sent to the ADP via a synchronous serial link with a speed of 0.1 μs bit^{-1} or 1 μs pixel^{-1}. By using the difference of the two samples, the reset noise of the CCD is essentially eliminated. In order to have the full resolution on the 10-bit range of the digital system, the integration time is currently programmed to be $\approx$ 700 μs as described by Fivian, Henneck, and Zehnder (2002). Beside the normal operational mode, several test and diagnostic modes (first-level modes) are implemented in the front-end FPGA.

On the ADP, the SAS data are processed first by a hardware program in the second-level FPGA (SAS/RAS FPGA) and then by the software running on the Data Signal Processor (DSP). For every SAS cycle (i.e., every 8 ms), the three measured solar profiles are stored in the SAS/RAS memory on the ADP. At the same time, while the data are flowing through the FPGA logic, the addresses of all trigger level transitions are stored. The trigger levels are programmable and

are stored in a FPGA register. In order to minimize the data rate consistent with the required pointing accuracy, a cadency divider is implemented which produces SAS interrupts to the DSP program with 128, 64, 32, 16, or 8 Hz. The nominal operational cadency of 32 Hz results in an additional pointing error of the order of 0.05 arc sec for linear interpolation between the measured points. However, the limited telemetry rate and a photon count rate that is higher than expected prior to launch required a reduction of the cadency to 16 Hz for a substantial fraction of operation time adding an error of ≈ 0.2 arc sec. An overview of the ADP software is given in Section 2.3.

2.2. ROLL ANGLE SYSTEM (RAS)

The RAS is a star scanner pointing radially outwards with respect to the rotating spacecraft and observes stars within a field of view of 60 to 90 deg in polar angle. Stars within the field of view are focused by a $f/1.4$ lens system with a focal length of 50 mm. While the spacecraft is rotating, the images of the stars travel over a linear CCD array and trigger one or several pixels. Even though the sensor is a TDI CCD (Time Delay and Integration CCD) with 2048×96 pixels with a pixel size of 13×13 μm^2, it is operated in a mode which makes it equivalent to a linear CCD with 2048 pixels with a size of 13×1248 μm^2 each. Thus, the field of view in roll angle is ≈ 1.4 deg. Assuming a rotational speed of 15 rpm, the passage time of a star event is between 15.3 ms and 17.6 ms depending on the polar angle with respect to the rotation axis. The size of a pixel corresponds to 0.9 arc min in polar angle.

The combined system with the optics and the CCD shows a spectral responsivity between 4000 Å and 10 000 Å with a maximum around 7000 Å. Thus, the sensitivity for a star detection depends strongly on its spectral type. The system is about twice as sensitive to M-class stars than to B-class stars. Although the integration time is programmable, the currently configured integration time is ≈ 8.8 ms corresponding to ≈ 47 arc min in roll angle. For a star with visual magnitude $m_V = 3$, this results in a response of 3.3 mV for a B0 star and 7.2 mV for a M0 star.

The front-end electronics with the first-level FPGA is very similar to that of the SAS with the difference that the cycle time is the same as the integration time which means that the CCD is always integrating light. The integrated charge is shifted out through the CCD shifter and digitized on a 12-bit ADC providing a resolution of 0.5 mV channel^{-1}. A double sampling and subsequent subtraction essentially eliminates the reset noise as described in Section 2.1. The timing for shifting the signals is the same as for the SAS. Besides the normal operational mode, several test and diagnostic modes (first-level modes) are implemented in the front-end FPGA.

As with the SAS subsystem, the RAS data are processed first by a hardware program in the second-level FPGA on the ADP and then by the software running on

the DSP processor. In Section 2.3 an overview of the ADP hardware and software is given. Nevertheless, the RAS relevant part of the second-level FPGA is described in the following two paragraphs.

At the same time as the data are flowing through the second-level FPGA logic, the addresses for all pixel values exceeding their individually programmable threshold values are stored. It has been shown by Fivian, Henneck, and Zehnder (2002), that a threshold of about 5 channels above the dark signal is marginal to trigger at least one star for every revolution of the spacecraft. Therefore, a pixel summation algorithm has been implemented in order to increase the signal to noise ratio. The FWHM of the point spread function is ≈ 2.6 pixels as pointed out by Zehnder *et al.* (2002) and Fivian, Henneck and Zehnder (2002). Thus a summation of two adjacent pixels combined with an adjusted threshold level provides an increase of a signal to noise of almost $\sqrt{2}$. Another factor of almost $\sqrt{2}$ can be gained by summing two temporal consecutive values of the same pixel number since the passage time of an event is almost double the integration time.

The low altitude orbit of RHESSI implies that almost 2π of the celestial sphere may be covered by the Earth. The signal induced by the Earth albedo can reach a level of 1000 times the saturation level of the RAS. Many CCD chips provide an anti-blooming feature, i.e. an internal chip capability to let the extra charge flow through an additional gate. However, the selected CCD in the RAS does not have that feature and therefore an extra mechanism had to be implemented. On the first-level FPGA, a programmable earth albedo threshold is set. If 64 pixels of a CCD readout are above this threshold value, the sensor is switched to maximum cadence of ≈ 2.2 ms per cycle and once the readout level is below the threshold again, the sensor is kept in this fast readout mode for a programmable additional time before being switched back to normal mode. This results in an additional blind time after rotating out of the Earth albedo of up to 0.8 s. Nevertheless, the flight data shows a change of the dark signal of several channels for many configurations of the Earth albedo with respect to the spacecraft. This causes many false trigger events which can be removed with the analysis software.

2.3. Aspect data processor (ADP)

The ADP controls the SAS and RAS front-ends, does on-board processing of CCD images and manages the data transfer between the front-ends and the Instrument Data Processing Unit (IDPU) (Curtis *et al.*, 2002). The processing is necessary in order to reduce the data rate since the aspect sensors generate ≈ 2 Mb s^{-1} of raw data and the data has to be formatted into telemetry packets to be read by the IDPU. The achieved data reduction is in the order of a factor of 1000. The ADP can be separated into three different hardware parts. In Figure 1 the three columns of units represent the SAS/RAS interface, the central processor and the communication control. The different parts including the software can be controlled by parameters which have to be loaded into the memory prior to running the software.

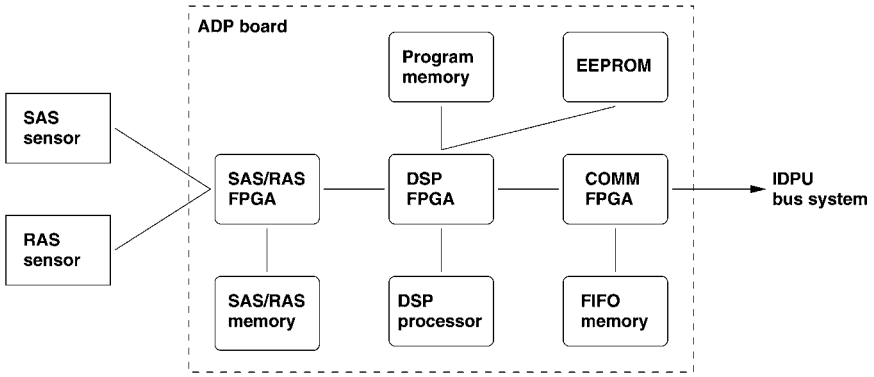

Figure 1. Simplified logical scheme of the Aspect Data Processor (ADP). For description see text in Section 2.3.

After initialization, the SAS/RAS interface acts as an independent unit and becomes responsible for the functioning of the SAS/RAS front-ends. The FPGA program which is driven by an internal sequencer is essentially described in Sections 2.1 and 2.2. It generates an interrupt to the central processing part for every SAS and RAS image which has been processed.

On the central processing unit, a DSP program processes the SAS and RAS data and generates basically four different classes of data to be stored in the FIFO. RAS star events, SAS limbs and SAS/RAS images are handled as different data streams. Whereas the images have to be formatted into telemetry packets only, the event-driven data from the SAS and the RAS need more processing. Images are stored frequently with a programmable duty cycle for later control of the gain and the dark signal.

In order to store the information for the solar limbs, the address and a programmable number of pixels for each limb are written to the telemetry packet. For every SAS cycle, all triggers from the first subsystem are stored first followed by the second and the third. The number of stored pixels above and below the threshold level can be programmed separately. It turned out that $2 + 2$ pixels is a optimum number to reach the required accuracy. For later analysis of the pointing, the cycles have to be counted in order to reconstruct the timing. The full resolution of 10 bits and a reduced resolution of the 8 most significant bits can be commanded.

Each RAS event consists of a time stamp, the address of the triggering pixel and a number of pixel values. For later reconstruction of the dark signal, a programmable number of pixels on either side of the pixels above threshold are stored. In general, a star event triggers several adjacent pixels which are treated as one event. Also with temporal and spatial summation enabled, the measured pixel values are stored for later analysis.

The third part of the ADP, the communication control, provides an interface between the DSP processor, the FIFO memory and the IDPU bus system. In addition, it stores the spacecraft time and incorporates power control.

A full list of all programmable parameters and a full list of the used APP-IDs (application identification numbers) identifying the different data streams are presented by Fivian (2002).

3. Reconstruction of the Aspect Solution

The telescope-fixed or spacecraft-fixed imaging coordinate system has been defined in such a way that any geometrical error has the least effect to the image reconstruction. Therefore, it has to be closely related to the features of the collimators and the SAS. The imaging $\tilde{z}$-axis or 'Imaging Axis' is defined to be parallel to the line from the center of gravity of the CCD centers to the center of gravity of the optical centers of the lenses. The origin is the center of gravity of the CCD centers and the sense of the $\tilde{z}$-axis is positive towards the Sun. Furthermore, the $\tilde{x}$- and $\tilde{y}$-axis are chosen to build a right-handed Cartesian coordinate system where the orientation of the $\tilde{y}$-axis is basically arbitrary. However, the $\tilde{y}$-axis is pointing approximately towards SAS10, the first SAS subsystem and is well defined with respect to the RAS defining the roll angle. All features from the front and rear grids, the SAS, the RAS and the PMTRAS have to be given in that coordinate system.

As indicated in Section 1 and described in detail by Hurford *et al.* (2002), the pointing of the rotating spacecraft and the roll angle have to be known at any given time in order to reconstruct images. A set of a well-defined pointing and roll angles is defined as the aspect solution. Figure 2 shows a instantaneous relation between the solar limb with solar-fixed xy-coordinates and the projection of the imaging $\tilde{x}\tilde{y}\tilde{z}$-coordinate system onto the Sun. The direction of the imaging $\tilde{z}$-axis is marked as 'Imaging Axis'. The pointing $\mathbf{P}_{\mathrm{ASPECT}}$ is defined to be the angle between the direction from the spacecraft towards the Sun center and the imaging axis. Furthermore, the roll angle φ is defined as the angle between the solar fixed y-axis and the projection of the spacecraft fixed imaging $\tilde{y}$-axis. The sign of the roll angle is defined to increase with time. From the spacecraft looking towards the Sun, the spacecraft is rotating clockwise, and therefore, a positive roll angle is a rotation from the solar y-axis towards the rotating $\tilde{y}$-axis as indicated in Figure 2.

Since the SAS is a part of the telescope mounted as close as possible to the grids, the solar pointing origins from the measurement of the position of the Sun center in the body frame. This vector is the same as the vector $\mathbf{P}_{\mathrm{ASPECT}}$ in Figure 2 with the opposite sign, but measured in the rotating $\tilde{x} - \tilde{y}$ imaging coordinate system. Let $\mathbf{P}_{\mathrm{SAS}}$ be the direction of the Sun center measured by the SAS and $\mathbf{P}_{\mathrm{ASPECT}}$ the solar pointing of the telescope as defined earlier in this section, then the transformation is as follows:

$$\mathbf{P}_{\mathrm{ASPECT}} = \begin{pmatrix} \cos\varphi & -\sin\varphi \\ -\sin\varphi & -\cos\varphi \end{pmatrix} \mathbf{P}_{\mathrm{SAS}}, \tag{1}$$

where φ is the roll angle. The matrix of the inverse transformation is identical.

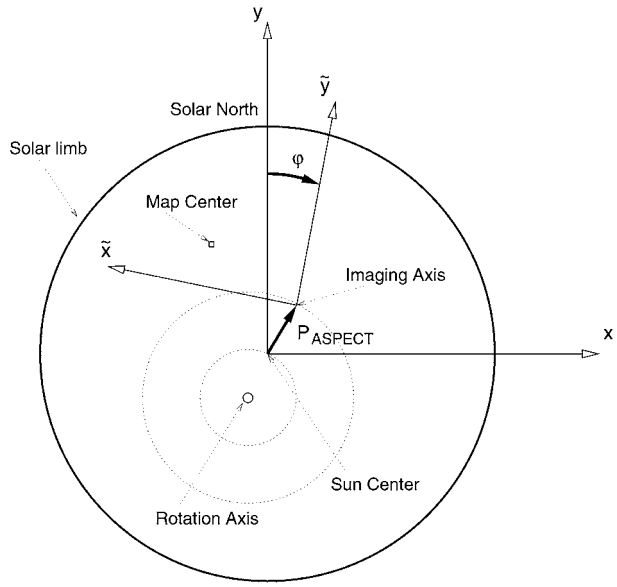

Figure 2. The *solid circle* represents the solar limb and the $x - y$ coordinate system refers to solar coordinates with the y-axis pointing toward solar north. At a given time, the telescope axis may point at any point on this projection plane. That point is marked with 'imaging axis' and the $\tilde{x} - \tilde{y}$ axis represents the spacecraft fixed coordinate system. The pointing of the spacecraft is defined as the angle between the Sun center and the imaging axis and is represented by the vector $\mathbf{P}_{\mathrm{ASPECT}}$. The roll angle φ is defined as the angle between the solar fixed y-axis and the projection of the spacecraft fixed $\tilde{y}$-axis.

3.1. THE SOLAR POINTING

The transmitted data of each of the six solar limbs are processed off-line by the aspect reconstruction software which is integrated in the ground based RHESSI data analysis software (Schwartz *et al.*, 2002). First the position on the CCDs for each limb is determined. For every given SAS cycle of transmitted solar limbs, the mid-perpendiculars to the straight lines between the two limb positions are constructed as shown schematically on the left part of Figure 3. In order to correlate the results from the three independent subsystems, conceptually the three systems are linearly shifted to share the point of the Sun center as shown on the right side of Figure 3. For ideal circumstances the mid-perpendiculars would then intersect in one point, the instantaneous position of the Sun center.

In general, the mid-perpendiculars form a residual triangle as indicated in Figure 4 and the center of gravity of the intersections is the best guess for the position of the Sun center. Hence, the solar pointing for every SAS cycle is determined and the high cadence of measurements allows linear interpolation to determine the solar pointing for any given time.

This reconstruction suffers from two main error sources. One is resulting from errors in the fit of the limb positions and the other is due to uncertainties in the

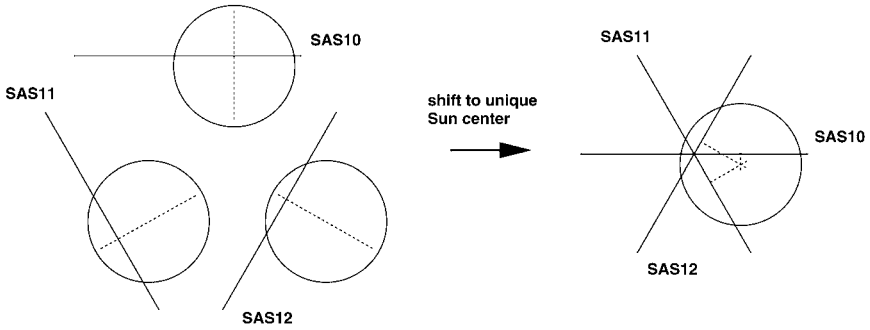

Figure 3. The CCD with the focused solar limb is shown for each subsystem *on the left part* of the schematic figure. Shifting the coordinates to share the point of the Sun center leads to the reconstruction of the instantaneous Sun center.

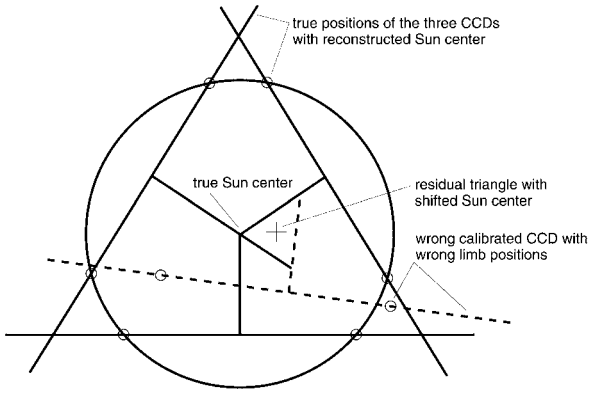

Figure 4. The *circle* indicates the solar limb and the *solid lines* are at the true positions of the CCDs with the corresponding reconstruction of the Sun center. A wrong calibration of the position of a CCD leads to a residual triangle in the reconstruction and therefore a shifted, incorrectly reconstructed Sun center as shown with the *dashed lines*.

knowledge of the geometry of the imager, therefore implying errors in correlating the three subsystems. If the fit of the limb positions had a systematic error, they would have the opposite sign for the positions of the two limbs on each of the CCDs. Thus, by calculating the mid-point of the two limb positions this error cancels essentially. The analysis of the flight data show that a linear fit of the pixel values and a subsequent fixed thresholding is accurate enough as pointed out later in this section.

The second source of pointing errors is a consequence of dimensional uncertainties. It can be well controlled by applying a self-calibration algorithm as described in detail by Fivian, Henneck and Zehnder (2002). In Figure 4, the case with an error for only one subsystem is represented. For the general case with a remaining residual triangle, the statistics of $1/\sqrt{3}$ of the length of the residual triangle or 2/3 of its height (Fivian, 2002), is a measure for the relative pointing error. Figure 5 shows the result for a typical orbit. Apparently, the spacecraft shows an off-pointing

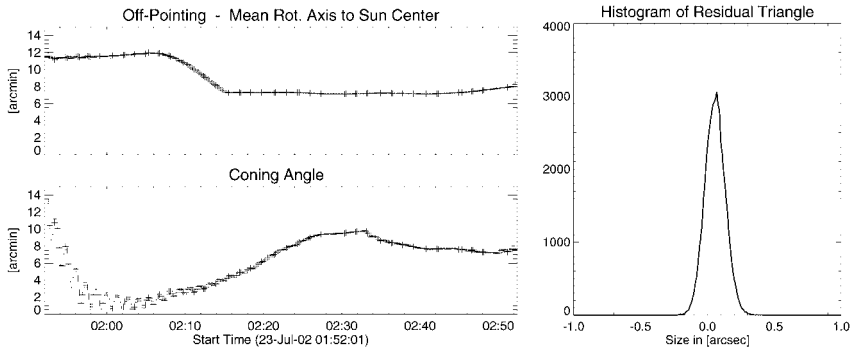

Figure 5. The plots show data for a typical orbit with the spacecraft being in direct sunlight. After sunrise, the spacecraft is pointed off the Sun center by ≈ 11 arc min and has a coning angle of ≈ 14 arc min, i.e., the rotation axis differs from the imaging axis. The angular momentum applied by the torque rods induces a precession which can be seen as wiggles in the coning angle for about 20 min. The complicated dynamics of changing the off-pointing and coning angle by several arc min is perfectly measured by the SAS, which is illustrated by plotting the histogram of the residual triangle for the same time range. The mean of the characteristic size of the residual triangle is ≈ 0.06 arc sec and the width of the distribution corresponds to $\sigma \approx 0.08$ arc sec. An additional error induced by interpolating measured data points adds to the given value (see Section 2.1).

from the Sun center of up to 12 arc min and a coning angle of up to 10 arc min. The latter is the angle between the imaging axis and the instantaneous rotation axis. With the current calibration the systematic error of the relative pointing is ≈ 0.06 arc sec and the statistical error is in the order of $\sigma \approx 0.08$ arc sec.

An overall shift or rotation of the imaging coordinates is called the absolute error of the solar pointing. Even though this can be seen as a cross-calibration between the SAS and the collimators, the calibration of the grid parameters corrects for initial mis-alignment. This calibration is based on 'focusing' the X-ray image by modifying the relative grid phases and keeping the imaging coordinates unchanged. In principle one can say, that any calibration error contributes to a blur of the X-ray image. The relation between the SAS and the grids is not fully understood yet. Nevertheless, images with a resolution of the order of 2–3 arc sec have been achieved.

3.2. THE ROLL ANGLE

The basic RAS principle is to determine the momentary roll orientation of the spacecraft with respect to known stars. In the rotating plane the roll angle determination can be reduced to a time measurement. Every star event contains several pixel values from the same CCD readout. In a first step, a Gaussian with an arbitrary baseline is fitted determining the polar angle, the dark signal and the response of that particular event. The response depends on the brightness of the star, its spectral type and the fraction of the integration time the star illuminated the CCD. Since the integration time is about two times shorter than the star passage time, a star event

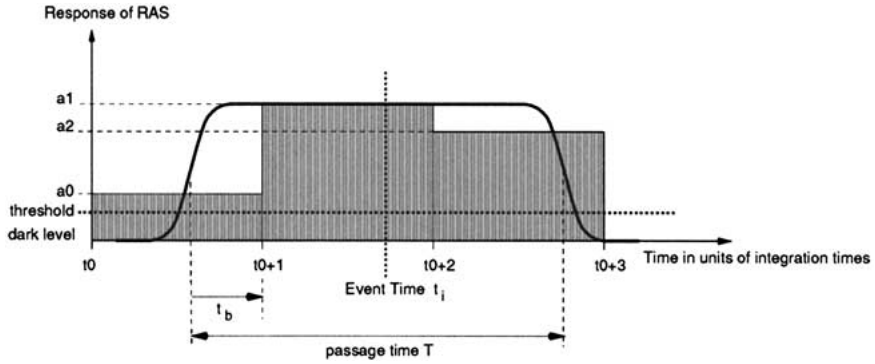

Figure 6. The *solid line* shows the response of the RAS CCD as a continuous function of time. Integration over a fixed time interval gives a histogram like function (*shadowed rectangles*) with values a_0, a_1, and a_2 for the integration cycles starting at t_0. After every integration time, the response level is compared to a threshold level for triggering the readout of the CCD pixels. The amplitudes a_i and the triggering time t_0 defines the temporal centroid t_i of the event.

generates a response on more than one consecutive time frame as represented in Figure 6. Thus, the problem has been reduced to a precise determination of the timing of a star event and the identification of an event with a specific star.

Assuming that the time dependency of the incident light for a star event can be treated as a function which is comparable to a rectangular shape. The width (FWHM) of the point spread function of the RAS optics is ≈ 2 arc min and this angle corresponds to ≈ 0.4 msec given the rotational speed of 15 rpm. Therefore, the convolution of the point spread parameterized in time with a rectangular function of the width of ≈ 15 msec passage time gives a small enough rise time.

Hence, the timing of a star event can be described by the equation system

$$a_0 = r t_b, \tag{2}$$

$$a_1 = r t_{\text{int}}, \tag{3}$$

$$a_2 = r(T - t_{\text{int}} - t_b), \tag{4}$$

which is made evident with Figure 6. For $i = 0, 1, 2$, a_i are the fitted responses for the particular time frames, r is the responsivity of the system, t_b is the time since the star entered the field of view to the next integration time, T is the passage time of a star event and t_{int} is the integration time. With a fully calibrated system and an identified star event, the equation system over-defines the only unknown t_b. The event time for that particular event is then $t_i = t_0 + t_{\text{int}} - t_b + T/2$.

The measured responses a_0, a_1, and a_2 have noise. Assuming that a_0 and a_2 have the same accuracy, t_b can be calculated in a symmetric way according to Equation (5) and the responsivity r can be calibrated by the statistics from many stars using $r = a_1/t_{\text{int}}$:

$$t_b = \frac{1}{2}\left(\frac{a_0 - a_2}{r} + T - t_{\text{int}}\right). \tag{5}$$

In order to achieve an accurate enough timing using Equation (5), the responsivity r has to be well calibrated and the passage time T has to be known. Since the responsivity depends on the star, it is basically unknown until the star has been identified but the sum of Equations (2)–(4) gives an initial estimate using $r = (a_0 + a_1 + a_2)/T$ leading to a timing according to Equation (6):

$$t_b = \frac{1}{2}\left(\left(\frac{a_0 - a_2}{a_0 + a_1 + a_2} + 1\right) T - t_{\text{int}}\right). \tag{6}$$

On the other hand, the passage time T is initially unknown and it has to be estimated using the statistics from a bigger number of star events. Once the responsivity and the passage time are estimated, the stars can be identified by comparing the timing, polar angle and the response with a star catalog. The RAS specific responsivity can be calibrated and stored in the star catalog too. Thus, after identifying the star events the responsivity is known and the estimate of the passage time can be improved with

$$T = \frac{a_0 + a_1 + a_2}{r}. \tag{7}$$

Hence, the calculation of the timing has to be done twice, first to achieve good estimates in order to identify the star events and second to result in an accurate timing.

For fainter stars, the response of the first and the last time frame might be too low to trigger RAS pixels. If only one of those is available, Equation (5) can be used in an asymmetrical way with only a_0 or a_2. If a star event results in pixels for only one time frame starting at t_0, the best estimate for the timing is simply $t_i = t_0 + t_{\text{int}}/2$.

The analysis and its software for the RAS aren't completed yet. The current status of the calibration is presented by Fivian, Henneck, and Zehnder (2002). However, the aspect reconstruction software currently uses the PMTRAS system to determine the roll angle. This system was designed as a backup roll angle system and is described by Hurford and Curtis (2002).

Acknowledgements

The authors thank Gordon Hurford, Peter Ming and the PSI workshop and design office for their substantial work on the design, building and integration of the hardware. This work has partially been funded by the Swiss National Science Foundation.

References

Curtis, D. W. *et al.*: 2002, *Solar Phys.*, this volume.
Fivian, M.: 2002, Thesis ETH.
Fivian, M., Henneck, R., and Zehnder, A.: 2002, *SPIE Proc.* **4853**, Waikoloa, Hawaii.
Hurford, G. J. and Curtis, D.: 2002, *Solar Phys.*, this volume.
Hurford, G. J. *et al.*: 2002, *Solar Phys.*, this volume.
Lin, R. P. *et al.*: 2002, *Solar Phys.*, this volume.
Schwartz, R. A. *et al.*: 2002, *Solar Phys.*, this volume.
Smith, D. M. *et al.*: 2002, *Solar Phys.*, this volume.
Zehnder, A. *et al.*: 2002, *SPIE Proc.* **4853**, Waikoloa, Hawaii.